which $Rh(acac)_3$-derived ions can form metal–carbon and metal–hydrogen bonds is certainly consistent with the well-known catalytic activity of reduced-valence rhodium compounds.

One minor process is worth noting because of its relationship to the mass spectrum of $Ru(acac)_3$ discussed below. $Rh(acac)_2^+$ loses 40 mass units to produce an ion with m/z 261 by loss of a purely hydrocarbon fragment (C_3H_4). The composition of this oxygen-free fragment is confirmed by the deuteration experiment. The resulting ion then loses CO_2 to become $Rh(acac)CH_3$ (m/z 217).

Tris(2,4-pentanedionato)ruthenium(III), Ru(acac)$_3$. The predominant ions in the mass spectrum of $Ru(acac)_3$ include the molecular ion, $Ru(acac)_3^{+\cdot}$, $Ru(acac)_2^+$, and CH_3CO^+. The remaining more intense ions (relative intensity greater than 15% of the base peak) are accounted for by the reaction sequence mentioned in the previous paragraph for $Rh(acac)_3$. Instead of a minor process, however, the sequence of the loss of C_3H_4 from $Ru(acac)_2^+$ to yield $Ru(acac)(CH_3)(CO_2)^+$ (m/z 260) followed by the loss of CO_2 to yield $Ru(acac)CH_3^+$ (m/z 216) is a relatively important reaction sequence entirely supported by the observation of peaks corresponding to metastable transitions (Scheme V). The assigned compositions are further supported by the mass spectrum of the partially deuterated $Ru(acac)_3$.

The remainder of the mass spectrum of $Ru(acac)_3$ is characterized by a number of less intense multiplets in the mass range of 120–200. These multiplets appear to correspond to the hydrocarbon-containing fragments noted in Table II for $Rh(acac)_3$. Because of their relatively low intensities, we have not attempted to assign compositions. The task is considerably complicated by the multiisotope nature of Ru and the one or two hydrogen atom difference separating some of these ions.

Summary

Both rhodium and ruthenium appear to play an important role in facilitating internal rearrangement in the complexing ligands. Such rearrangements seem likely to occur via the formation of bonds between the metal center and portions of the ligand, e.g. F., CO, CH_3, and H. The main difference between the two metals is the stability of the metal–(small fragment) bond. Ruthenium binds irreversibly (in the context of the mass spectrometric experiment) to F and CH_3, and the free metal ion is not osberved. Bonds to rhodium, on the other hand, appear more easily made and broken, and numerous metal-containing species develop as well as the free Rh(I) ion. The ease of making and breaking bonds to rhodium would seem to be an important aspect of its well-known catalytic activity.

Acknowledgment. The authors thank Mark A. Carlson for obtaining the mass spectra discussed above.

Registry No. $Rh(acac)_3$, 14284-92-5; $Rh(tfa)_3$, 14652-54-1; $Rh(hfa)_3$, 14038-71-2; $Ru(acac)_3$, 14284-93-6; $Ru(tfa)_3$, 16702-38-8; $Ru(hfa)_3$, 16827-63-7.

Contribution from the Department of Chemistry, University of Pittsburgh, Pittsburgh, Pennsylvania 15260

Mössbauer Study of Imidazole and N-Heterocyclic Complexes of Pentacyanoiron(II) and Pentacyanoiron(III)

CRAIG R. JOHNSON and REX E. SHEPHERD*

Received March 8, 1983

The Mössbauer spectra of $(CN)_5Fe^{II}L^{3-}$ and $(CN)_5Fe^{III}L^{2-}$ salts have been obtained for L = a series of imidazoles, pyrazoles, pyridines, and pyrazines. The Fe(II) complexes of the imidazoles behave normally with center shifts close to 0.29 mm/s and quadrupole splittings, Δ, equal to 0.65 mm/s (1-methylimidazole) to 0.87 mm/s (*l*-histidine). A plot of the $^1E_{(1)} \leftarrow {}^1A_1$, d–d transition energy vs. the center shift is linear, both quantities related to $\sigma + \pi$ effects on the bonding. The imidazoles are shown to fall on a line established by "σ-only" ligand donors, while pyridines and pyrazines fall off the line of positive slope and to the right when center shift ($\sigma + \pi$ parameter) is plotted vs. quadrupole splitting, a $\sigma - \pi$ parameter. Thus, imidazoles are shown to be very weak π acceptors compared to the more aromatic heterocyclic ligands, whose complexes also exhibit well-defined metal-to-ligand charge-transfer (MLCT) bands. The Fe(III) complexes are studied in detail here for the first time. Golding's predicted upper limit to Δ of 2.54 mm/s for $(CN)_5FeL^{2-}$ ions with large distortions from octahedral symmetry has been experimentally demonstrated. Ligands are found to influence Δ for $(CN)_5FeL^{2-}$ complexes as two distinct sets of ligands. For heterocyclic rings containing an additional nonbonding lone pair either internal or exo (and resonant) with the ring, Δ approaches Golding's limit. The value of Δ is almost independent of the σ strength of L over 7 pK_a units. The same set of complexes possess a ligand-to-metal charge-transfer (LMCT) band in the visible electronic region. Ligands meeting these criteria include the imidazoles, benzimidazole, pyrazoles, and aminopyridines. This group must be better π donors than CN^-. By contrast, heterocyclic rings with no internal or exo nonbonding lone pairs produce $(CN)_5FeL^{2-}$ complexes with no LMCT band and have Δ values approximately proportional to the σ donor strength of L as estimated by protonic pK_a's. The center shifts of the Fe(III) complexes vary between 0.11 and 0.20 mm/s; the differences are mostly due to variation in the cation from Ca^{2+}, Zn^{2+}, Na^+, and *N*,*N*′-dimethyl-1,4-diazoniabicyclo[2.2.2]octane ion.

Introduction

A number of physical, thermodynamic, and kinetic properties of imidazole and imidazolate complexes of pentacyanoiron(II) and -iron(III) have been reported by our laboratory[1,2] and by others.[3-5] For the Fe(III) complexes, $(CN)_5FeL^{2-}$, a ligand-to-metal charge-transfer (LMCT) band is observed with N-heterocyclic ligands, L, that have lone pairs in addition to the bonding lone pair at N. We have examined the low-spin Fe(II) and Fe(III) complexes of a series of N-heterocyclic complexes with the goal of evaluating aspects of the bonding to N-heterocyclic ligands, in particular the imidazole family, by means of Mössbauer-effect spectroscopy. A significant amount of literature exists for the Mössbauer

(1) Johnson, C. R.; Shepherd, R. E.; Marr, B.; O'Donnell, S.; Dressick, W. *J. Am. Chem. Soc.* **1980**, *102*, 6227–6235.
(2) (a) Shepherd, R. E. *J. Am. Chem. Soc.* **1976**, *98*, 3329–3335. (b) Bowers, M. L.; Kovacs, D.; Shepherd, R. E. *Ibid.* **1977**, *99*, 6555–6561.
(3) Toma, H. E.; Batista, A. A.; Gray, H. B. *J. Am. Chem. Soc.* **1982**, *104*, 7509–7515.
(4) Toma, H. E.; Martins, J. M.; Giesbrecht, E. *J. Chem. Soc., Dalton Trans.* **1978**, 1610–1617.
(5) Szecsy, A. P.; Haim, A. *J. Am. Chem. Soc.* **1981**, *103*, 1679–1683.

0020-1669/83/1322-3506$01.50/0

Table I. Mössbauer Data for $(CN)_5FeL^{3-}$ Complexes of Imidazole and Imidazole Derivatives, $M_x(CN)_5FeL \cdot XH_2O$[a]

ligand (L)	cation (M)	center shift (δ), mm/s	quadrupole splitting (Δ), mm/s
imidazole	K^+	0.29	0.77[b]
1-methylimidazole	K^+	0.28	0.65
2-methylimidazole	K^+	0.30	0.79
4-methylimidazole	K^+	0.29	0.75
l-histidine	Na^+	0.28	0.87
benzimidazole	Na^+	0.28	0.75
hypoxanthine	Na^+	0.28	0.72
4-nitroimidazole	K^+	0.30	0.67
imidazole	$(NH_3)_5Co(imz)^{3+}$	0.27	0.75
imidazole	$Ru(NH_3)_6^{3+}$	0.26	0.83
2-methylimidazole	$Co(NH_3)_6^{3+}$	0.26	0.80

[a] NP reference standard; δ is ±0.02 mm/s. [b] Line width = 0.47 mm/s at half-height.

spectra of pentacyanoiron(II) complexes. However, the case for the Fe(III) analogues is surprisingly limited. Mössbauer spectra for these complexes with aromatic N-heterocycles are reported here for the first time. A theoretical treatment by Golding has predicted that the maximum quadrupole splitting for $(CN)_5FeL^{2-}$ complexes should be 2.54 mm/s.[6] This upper limit has not been demonstrated experimentally in any reported case. We present evidence that Golding's treatment is correct by the examination of the center shift and quadrupole splitting for a variety of N-heterocyclic complexes. It is assumed that bonding properties of CN^- do not change significantly and that changes in the Mössbauer parameters reflect the changes in bonding of L as L is varied.

Various physical methods have been used to study the bonding between Fe(II) and L in the $(CN)_5FeL^{3-}$ series, including UV–visible spectroscopy,[7] ^1H and ^{13}C nuclear magnetic resonance,[8] and cyclic voltammetry[9] in addition to Mössbauer spectroscopy. Of particular interest in these studies is an evaluation of the extent of π back-bonding from the filled metal t_{2g} orbitals (with octahedral symmetry assumed to the first approximation) to an unoccupied π^* orbital on L. Although Mössbauer data for a number of $(CN)_5FeL^{3-}$ complexes were obtained very early in the development of the technique, the measurements have recently been repeated with modern methods to provide an internally consistent data set.[10] This information is useful in evaluating the data obtained for the imidazole complexes.

Results

Low-Spin Fe(II) Series: $(CN)_5FeL^{3-}$ Complexes. The Mössbauer data for the imidazole complexes of $(CN)_5Fe^{II}$ 3- are shown in Table I. The center shift for $(CN)_5Fe(imz)^{3-}$ has been reported previously[11] as 0.28 mm/s in good agreement with the value of 0.29 mm/s obtained in this work. The center shifts for all of the various imidazole complexes reported are close to 0.29 mm/s. The center shifts for the entries in the table with the large counterions $Co(NH_3)_6^{3+}$, $Ru(NH_3)_6^{3+}$, and $(NH_3)_5Co(imz)^{3+}$ appear to be slightly less, but the difference may not be significant since the reproducibility of the measurements is considered to be ±0.02 mm/s. Line widths at half-height were about 0.47 mm/s for Fe(II) complexes. The Mössbauer spectrum of $K_3(CN)_5Fe(imz) \cdot 3H_2O$ is shown in Figure 1B. This spectrum is typical of all of the imidazole complexes. The quadrupole splitting shows more variation from complex to complex than does the center shift, covering a range of ±0.2 mm/s with 1-methylimidazole showing the smallest splitting and *l*-histidine the largest.

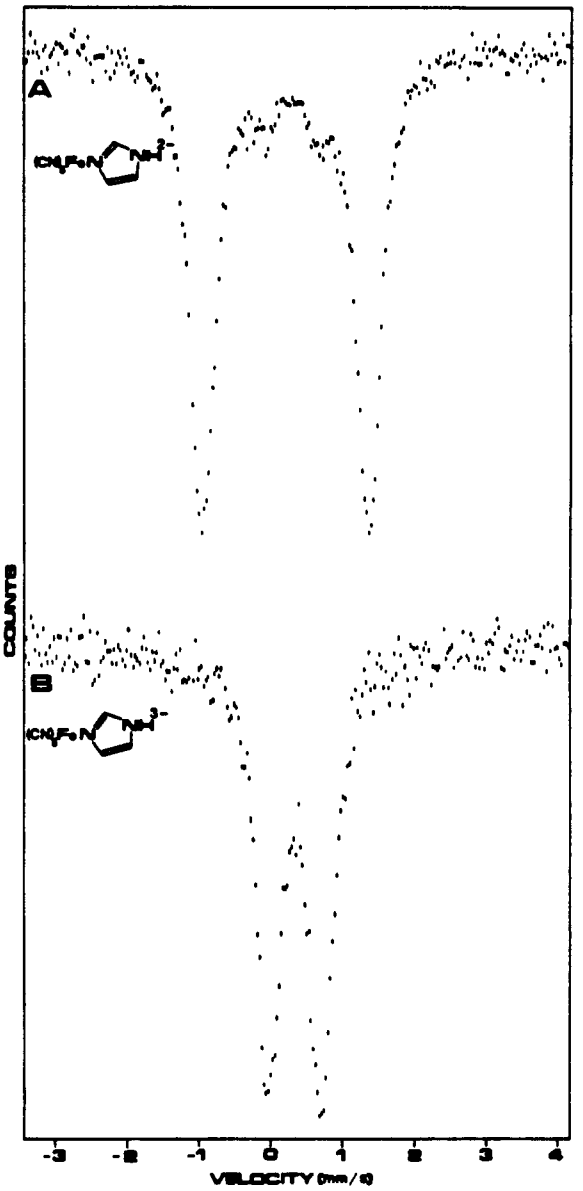

Figure 1. Comparison of the Mössbauer spectra of (A) Ca-$[(CN)_5Fe(imz)] \cdot XH_2O$ and (B) $Na_3(CN)_5Fe(imz) \cdot 3H_2O$. The small doublet in spectrum A is due to a small amount of the Fe(II) complex.

Low-Spin Fe(III) Series: $(CN)_5FeL^{2-}$ Complexes. A Mössbauer spectrum of $Ca(CN)_5Fe(imz)$ is shown in Figure 1A. In addition to the main doublet, another well-resolved, but much weaker, doublet is also observed. Comparison with Figure 1B indicates that this second doublet is due to a small amount of the Fe(II) complex in this particular sample. Other preparations of $Ca(CN)_5Fe(imz)$ did not show this feature in the spectrum, indicating that the complex was fully oxidized. The main doublet of this spectrum is typical of the complexes of $(CN)_5Fe^{2-}$ with the various imidazoles. The Mössbauer data for these complexes are shown in Table II. The various imidazole complexes have quadrupole splittings within the range of 2.2–2.55 mm/s. Line widths at half-height are about 0.43 mm/s for Fe(III) complexes. The Mössbauer spectra were originally obtained to ascertain if this technique was

(6) (a) Golding, R. M. *Mol. Phys.* **1967**, *12*, 13–23. (b) Golding, R. M. "Applied Wave Mechanics"; Van Nostrand: New York, 1969; Chapter 9.
(7) Toma, H. E.; Malin, J. M. *Inorg. Chem.* **1973**, *12*, 1039–1045.
(8) (a) Malin, J. M.; Schmidt, C. F.; Toma, H. E. *Inorg. Chem.* **1975**, *14*, 2924–2928. (b) Figard, J. E.; Paukstelis, J. V.; Byrne, E. F.; Petersen, J. D. *J. Am. Chem. Soc.* **1977**, *99*, 8417–8425.
(9) Toma, H. E.; Creutz, C. *Inorg. Chem.* **1977**, *16*, 545–550.
(10) Monaghan, C. P.; Fanning, J. C. *J. Phys. Chem.* **1978**, *82*, 1045–1051.
(11) Toma, H. E.; Vanin, J. A.; Malin, J. M. *Inorg. Chim. Acta* **1979**, *33*, L157–L159.

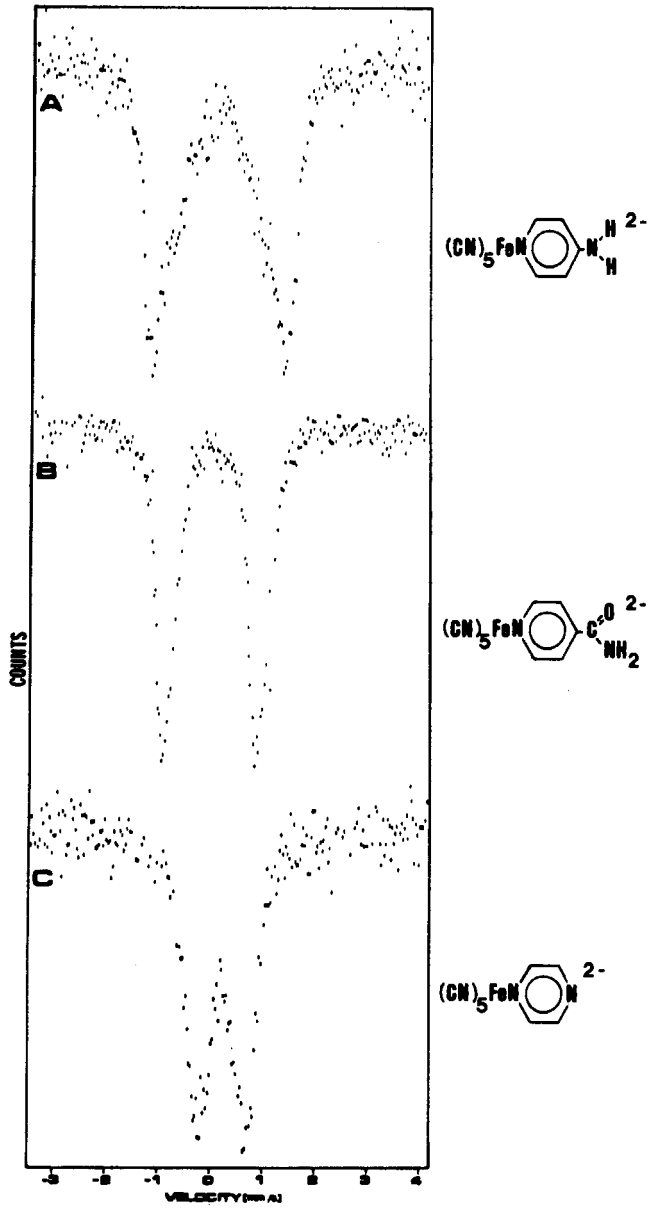

Figure 2. Mössbauer spectra of the Fe(III) complexes $Na_2[(CN)_5FeL]\cdot XH_2O$ where L = (A) 4-aminopyridine, (B) isonicotinamide, and (C) pyrazine.

sensitive enough to the nature of the ligand, L, to distinguish between imidazoles with different substituents. Although the quadrupole splittings vary as the substituents on the imidazole are change, the difference in the splitting is less than the change observed when the identity of the cation is changed.

The study was extended to other aromatic nitrogen heterocycles to see if their Mössbauer spectra differ from the imidazole results. The data for these complexes are also shown in Table II. The pyrazole and 3,5-dimethylpyrazole complexes of $(CN)_5Fe^{2-}$ have quadrupole splittings in the range of the imidazole complexes. With the exception of the 4-aminopyridine and 4-(dimethylamino)pyridine complexes, all of the pyridine complexes have quadrupole splittings that are smaller than the value for the imidazole complexes. A comparison of the spectra for the complexes of 4-aminopyridine, isonicotinamide, and pyrazine is shown in Figure 2. These complexes cover a wide range of quadrupole splittings: 0.9–2.5 mm/s. An examination of the data for the pyridine ligands in Table II reveals a general trend of decreasing quadrupole splittings with decreasing pK_a of the free ligand. The quadrupole splitting of these complexes is also sensitive to the nature of the cation as shown by the $(CN)_5Fe(py)^{2-}$ data with Ca^{2+}, Na^+, or $(CH_3)_2Dabco^{2+}$ as the counterion. The correlation between the quadrupole splitting of the $(CN)_5FeL^{2-}$ complex and the pK_a of the ligand (L) is shown in Figure 3. The data for the complexes of the azines and the pyridines were fit to a line by a linear least-squares program. These data are indicated by the solid points. Although several data points are fairly far from the line, a correlation between the quadrupole splitting and the pK_a is clearly evident. The data for the complexes of the imidazoles and pyrazoles are plotted as open data points. The complexes that have ligand-to-metal charge transfer (LMCT) transitions in the visible range are indicated by squares. The circles indicate that no LMCT transition is observed in the visible region for these complexes. Two distinct groups of data emerge from this plot: those with large quadrupole splittings (~2.5 mm/s) exhibiting LMCT transitions and those with smaller quadrupole splittings (<2 mm/s) exhibiting no LMCT transition in the visible region. The quadrupole splitting of the former group is independent of the pK_a of the ligand, while the latter group shows a roughly linear correlation with the pK_a of the ligand.

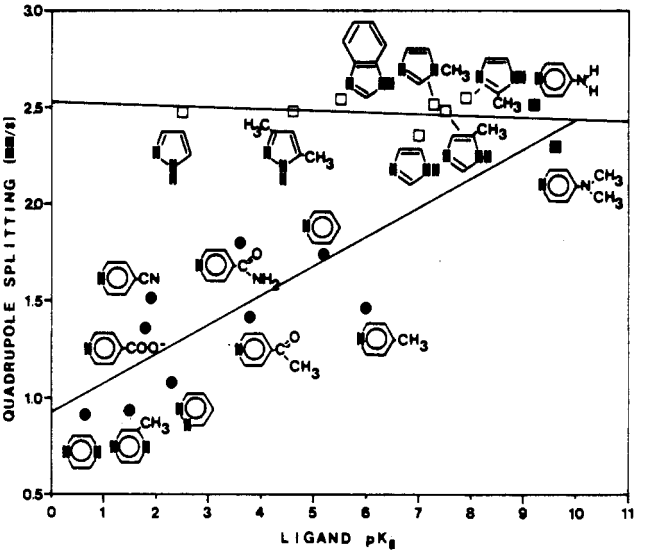

Figure 3. Correlation between the quadrupole splittings of the Fe(III) complexes, $(CN)_5FeL^{2-}$, and the pK_a of the free ligand, L. Solid points indicate "pyridine-like" ligands. Open points indicate "imidazole-like" ligands. Square points indicate that these complexes display low-energy LMCT transitions. Round points indicate that these complexes do not have low-energy LMCT transitions. One line is fit to the pyridine data. The other line is fit to the imidazole data.

Discussion

$(CN)_5FeL^{3-}$ Series. Toma et al. have demonstrated a correlation between the Mössbauer and UV–visible spectra for the $(CN)_5FeL^{3-}$ series.[12] The center shift from the Mössbauer spectrum and the crystal field splitting ($10Dq$), as evaluated from the UV–visible spectrum, are both sensitive to the $\sigma + \pi$ ability of L. The center shift should decrease and $10Dq$ should increase as the σ donor and/or π acceptor ability of the ligand increases. Evaluation of $10Dq$ from the UV–visible spectrum is difficult, however, because the d–d transitions are generally obscured by intense charge-transfer transitions from Fe(II) to the cyanide ligands and to L. If the local symmetry of the $(CN)_5FeL^{3-}$ complexes is considered to be C_{4v}, the ground state is $^1A_1$ and the low-energy excited states of the same multiplicity are $^1A_2$ and $^1E_{(1)}$. Thus, two d–d transitions are typically observed for such d^6 complexes—$^1E_{(1)} \leftarrow {}^1A_1$ and $^1A_2 \leftarrow {}^1A_1$. The $^1A_2 \leftarrow {}^1A_1$ transition is primarily a transition from d_{xy} to $d_{x^2-y^2}$ and should be relatively insensitive to the

(12) Toma, H. E.; Giesbrecht, E.; Malin, J. M.; Fluck, E. *Inorg. Chim. Acta* **1975**, *14*, 11–15.

Table II. Mössbauer Data for $(CN)_5FeL^{2-}$ Complexes[a]

ligand (L)	ligand pK_a	cation	center shift (δ), mm/s	line width, mm/s	quadrupole splitting (Δ), mm/s
		Imidazoles			
imz	7.0	Ca^{2+}	0.16	0.43	2.35
		Zn^{2+}	0.17		2.40
1-CH_3imz	7.3	Ca^{2+}	0.18	0.43	2.51
		Zn^{2+}	0.16		2.23
2-CH_3imz	7.9	Ca^{2+}	0.16	0.36	2.55
		$(CH_3)_2Dabco^{2+}$	0.19		2.32
4-CH_3imz	7.5	Ca^{2+}	0.16		2.48
1,2-$(CH_3)_2$imz		Ca^{2+}	0.18	0.43	2.34
benzimidazole	5.5	Na^+	0.18		2.54
		Pyrazoles			
pyz	2.5	Na^+	0.17		2.47
3,5-$(CH_3)_2$pyz	4.6	Na^+	0.17		2.47
		Pyridines			
4-$((CH_3)_2N)$py	9.6	Na^+	0.16		2.30
4-(NH_2)py	9.2	Na^+	0.18	0.66	2.51
4-CH_3py	6.0	$(CH_3)_2Dabco^{2+}$	0.18		1.46
py	5.2	Ca^{2+}	0.17	0.45	2.12
		Na^+	0.11	0.42	1.74
		$(CH_3)_2Dabco^{2+}$	0.19		1.46
4-C(O)CH_3py	3.8	$(CH_3)_2Dabco^{2+}$	0.18		1.41
4-C(O)NH_2py	3.6	Na^+	0.17	0.40	1.80
pyridazine	2.3	$(CH_3)_2Dabco^{2+}$	0.20		1.08
4-CH_3py	1.9	Na^+	0.19	0.40	1.51
4-COOHpy	1.8	Na^+	0.16	0.47	1.36
2-CH_3pz	1.5	Na^+	0.18	0.45	0.93
pz	0.65	Na^+	0.18	0.60	0.91

[a] NP reference standard; δ is ±0.02 mm/s. Abbreviations: imz, imidazole; pyz, pyrazole; py, pyridine; pz, pyrazine; Dabco, *N,N'*-dimethyl-1,4-diazoniabicyclo[2.2.2]octane.

Table III. Mössbauer and UV-Visible Data for $(CN)_5FeL^{3-}$ Complexes

ligand (L)	$E(^1E_{(1)} \leftarrow {}^1A_1)$, nm ($10^3$ cm^{-1})	liquid-N_2 temp δ, mm/s	liquid-N_2 temp Δ, mm/s	room temp δ, mm/s	room temp Δ, mm/s
NO^+	265 (37.8)[b]			0.0	1.712[c]
CO	306 (32.7)[b]			0.118	0.336[c]
CN^-	323 (31.0)[b,d]			0.192	0[c]
Me_2SO	351 (28.5)[b]	0.26	1.10[b]	0.226	1.028[c]
N-CH_3pz^+ [e]	380 (26.3)[b]	0.32	1.10[b]	0.262	0.964
histidine	381 (26.2)[a]			0.28	0.87[a]
imidazole	382 (26.2)[a]			0.29	0.77[a]
4-methylimidazole	383 (26.1)[a]			0.29	0.75[a]
2-methylimidazole	387 (25.8)[a]			0.30	0.79[a]
$pyCO_2^-$	386 (25.9)[b]	0.34	0.96[b]	0.26	0.80[a]
NH_3	398 (25.1)[b]	0.37	0.63[b]	0.285	0.694[c]
H_2O	442 (22.6)[b]	0.42	0.71[b]	0.297	0.795[c]

[a] This work. [b] Reference 12 (chemical shifts changed to NP reference). [c] Reference 10. [d] Energy of $^1T_{1g} \leftarrow {}^1A_{1g}$ transition. [e] *N*-CH_3pz^+ = *N*-methylpyrazinium ion.

identity of L along the *z* axis. The $^1A_2 \leftarrow {}^1A_1$ band is expected at ~320 nm (31×10^3 cm^{-1}) but is not observed due to electron-transfer bands in that region. The other d–d transition ($^1E_{(1)} \leftarrow {}^1A_1$) is only observed when it is not obscured by charge-transfer transitions from Fe(II) to L. This is the case when no charge transfer to L occurs in the visible region (e.g. when L = imidazole) or when the charge transfer to L is very low in energy (e.g. when L = *N*-CH_3pz^+). The energies of the $^1E_{(1)} \leftarrow {}^1A_1$ transition for the complexes considered by Toma et al.[12] and for the imidazole complexes discussed in this work are shown in Table III. The energy of this transition varies with the identity of L. Toma et al.[12] demonstrated that the energy of the $^1E_{(1)}$ transition gives a good linear correlation with the center shift for this series of substituted pentacyanoferrate(II) complexes. This is consistent with the $^1E_{(1)}$

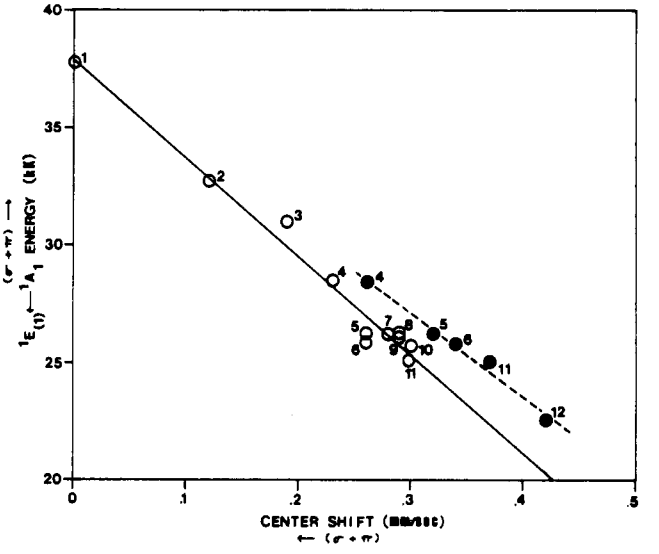

Figure 4. Correlation between the energy of the $^1E_{(1)} \leftarrow {}^1A_1$ d–d transition and the center shift for the $(CN)_5Fe^{II}L^{3-}$ complexes, L = (1) NO^+, (2) CO, (3) CN^- (4) Me_2SO, (5) *N*-methylpyrazinium, (6) isonicotinic acid, (7) histidine, (8) imidazole, (9) 4-methylimidazole, (10) 2-methylimidazole, (11) NH_3, (12) H_2O. Open points are room-temperature data. Solid points are data taken at liquid-nitrogen temperature.

$\leftarrow {}^1A_1$ energy being proportional to $10Dq$ and with the center shift and $10Dq$ being related to the $\sigma + \pi$ ability of the ligand, L. Figure 4 shows the plot of the energy of the $^1E_{(1)} \leftarrow {}^1A_1$ transition for these complexes vs. the center shift. As Toma et al. have shown,[12] the center shift data determined at liquid-nitrogen temperature give a good linear fit. A reviewer notes that room-temperature values of δ are related to values at liquid-nitrogen temperature by a fairly constant second-order Doppler shift. The lines drawn in Figure 4 were de-

termined by a linear least-squares procedure. The room-temperature center shift data also show a good linear correlation with the energy of the d–d transition. The least-squares fit gives a slope of −42.03 ± 2.34 and an intercept of 37.8 ± 0.6. The data for the $(CN)_5Fe^{3-}$ complexes of imidazole, 2-methylimidazole, 4-methylimidazole, and histidine fall on this line. This confirms the assignment of the ~385-nm absorption as the $^1E_{(1)} \leftarrow {}^1A_1$ (d–d) transition.

The UV–visible and Mössbauer data indicate that the imidazoles have a ligand field strength slightly greater than that for NH_3 despite their lower basicity based on proton affinity. The greater ligand field strength of imidazole (and smaller center shift) may be due to a small amount of back-bonding from the Fe(II) to the imidazole. When imidazole is complexed to the non-back-bonding moiety, $(NH_3)_5Co^{3+}$, the ligand field strength, as determined by the position of the d–d transitions, is essentially identical with that for NH_3.

Bancroft has shown that the σ donor and π acceptor abilities of ligands coordinated to low-spin Fe(II) may be qualitatively sorted out by evaluating the quadrupole splitting in relationship to the center shift.[13] For the closed-shell $(t_{2g})^6$ configuration, the main contribution to the electric field gradient will come from an unsymmetrical 3d electron density distribution due to L in the $(CN)_5FeL^{3-}$ complex. The quadrupole splitting arises from two parts, $q_{lattice}$ and $q_{valence}$. The lattice contribution is due to the external counterion charges. $q_{lattice}$ is neglected because it is small and presumably may be minimized by comparing only salts of cations of similar size, for example Na^+, K^+, etc. The $q_{valence}$ component, composed of q_{CF} and q_{MO}) for crystal field and covalent contributions, is predominantly q_{MO} for low-spin d^6 Fe(II) cyanides. q_{MO} reflects covalent bonding between the metal and ligands.

The primary consideration for the $(CN)_5FeL^{3-}$ series must be a comparison of the bonding properties of L and CN^-. If L is a better σ donor than CN^-, charge density is increased along the z axis (the NC–Fe–L axis) and a negative contribution to q_{MO} is expected. If L is a better π acceptor than CN^-, charge is delocalized along the z axis via back-bonding from d_{xz} and d_{yz} onto the ligand and a positive contribution to q_{MO} is expected. By this description, σ donation and π acceptance have opposing effects on the quadrupole splitting. The quadrupole splitting will become more positive with decreasing $\sigma - \pi$ ability. With use of magnetic field techniques, the sign of the quadrupole splitting has been shown to be positive for L = NO^+, NH_3, and H_2O.[14] The quadrupole splitting is believed to be positive in all cases, although this is less certain for L = CO. This indicates that these ligands are poorer σ donors and/or better π acceptors than CN^-.

Since the center shift is sensitive to the $\sigma + \pi$ ability of the ligand and the quadrupole splitting is sensitive to $\sigma - \pi$ ability, the center shift should show a linear correlation with the quadrupole splitting for those complexes where the σ donor ability of L predominates in influencing the value of the Mössbauer parameters; i.e., L has weak or no π acceptor ability and/or considerable σ donor ability. Bancroft has used a plot of center shift vs. the quadrupole splitting to separate out σ and π effects for a series of *trans*-$[FeHL(depe)_2]BPh_4$ complexes (depe = $Et_2PCH_2CH_2PEt_2$).[13] The same approach is used here for the $(CN)_5FeL^{3-}$ series. Some additional Mössbauer data that are useful in separating out the σ and π effects of L in this series are shown in Table IV. The Mössbauer data in Tables I and IV are used in Figure 5A to construct a plot of the center shift vs. quadrupole splitting. The data for $Fe(CN)_6^{4-}$ are not included in the plot since the hexacyano complex shows no quadrupole splitting. The line

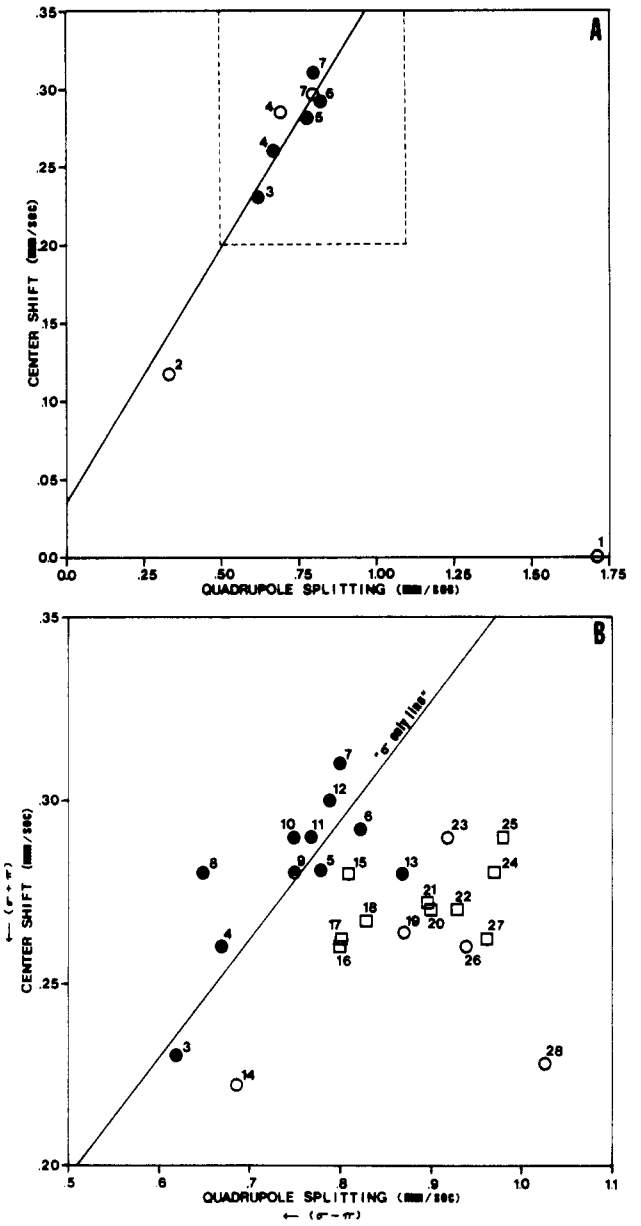

Figure 5. Correlation between the center shift and the quadrupole splitting for the $(CN)_5Fe^{II}L^{n-}$ complexes, L = (1) NO^+, (2) CO, (3) PPh_3, (4) NH_3, (5) NH_2CH_3, (6) $NH(CH_3)_2$, (7) H_2O, (8) 1-methylimidazole, (9) benzimidazole, (10) 4-methylimidazole, (11) imidazole, (12) 2-methylimidazole, (13) histidine, (14) SO_3^{2-}, (15) 4-cyanopyridine, (16) isonicotinic acid, (17) pyridine, (18) 4-methylpyridine, (19) NO_2^-, (20) isonicotinamide, (21) pyrazine, (22) 4,4′-bipyridyl, (23) $AsPh_3$, (24) 2,6-dimethylpyrazine, (25) 2-methylpyrazine, (26) $SbPh_3$, (27) *N*-methylpyrazinium ion, (28) Me_2SO. Round data points indicate complexes that do not have low-energy MLCT transitions. Square data points indicate complexes that exhibit MLCT transitions. Solid points indicate complexes used to define the "σ-only" line. Points 8–13 were excluded from the "σ-only" set; these are the complexes of the imidazole series of ligands. Part B is an expanded display of the region enclosed by the dotted line in part A.

shown in the plot was first determined with use of the data for ligands that are only capable of bonding with σ donation—L = H_2O, NH_3, NH_2CH_3, $NH(CH_3)_2$. This very limited set of data does not establish a very good linear correlation between the center shift and the quadrupole splitting. The range of quadrupole splitting and center shifts covered is too small for these σ-only ligands. Data are available for other aliphatic amine ligands, but the center shifts and quadrupole splittings are very close to the values for the amines

(13) Bancroft, G. M. "Mössbauer Spectroscopy"; Wiley, New York, 1973; Chapters 5 and 6.
(14) Reference 13, p 116.

Table IV. Additional Mössbauer Data for $(CN)_5FeL^{3-}$ Complexes

ligand (L)	center shift (δ), mm/s	quadrupole splitting (Δ), mm/s
NH_2CH_3	0.281	0.780[b]
$NH(CH_3)_2$	0.292	0.823[b]
PPh_3	0.23	0.62[c]
pyridine	0.262	0.802[b]
4-methylpyridine	0.267	0.830[b]
NO_2^-	0.264	0.872[b]
pyrazine	0.272	0.897[b]
SO_3^{2-}	0.222	0.687[b]
$AsPh_3$	0.29	0.92[c]
$SbPh_3$	0.26	0.94[c]
2-methylpyrazine	0.29	0.98[a]
2,6-dimethylpyrazine	0.28	0.97[a]
4,4'-bipyridine	0.27	0.93[a]
4-C(O)NH_2py	0.27	0.90[a]
4-CNpy	0.28	0.81[a]

[a] This work. [b] Reference 10. [c] Reference 13.

used here and do not contribute any useful new points to the plot. Using Bancroft's values for the complexes of NH_3 and H_2O,[13] as opposed to the more recently determined values,[10] improves the linear correlation and fits a line that also extrapolates near the data points for L = PPh_3 and CO. The line drawn in Figure 5B is the least-squares fit to the data for L = H_2O, NH_3, NH_2CH_3, $NH(CH_3)_2$, and PPh_3. These data are indicated by the solid circles. The inclusion of PPh_3 on this "σ-only" line is not unreasonable. The π acceptor ability of PPh_3 is expected to be slight at best,[15] and probably nil, when PPh_3 is forced to complete with CN^- for π electron density. Conversely, the fact that CO should fall near the "σ-only" line is quite surprising. If the data are not anomalous, this may indicate that, for low-spin Fe(II), CO is a moderate σ donor in addition to being a good π acceptor. In this respect CO is very much like CN^-. This observation is further supported by the small quadrupole splitting (0.336 mm/s) for CO—the smallest for any pentacyanoferrate(II) complex (if Δ is assumed to be positive). This suggests that the σ donor ability of CO, although poor, makes an appreciable contribution in determining the magnitude of quadrupole splitting of the complex. The Lewis basicity of CO is negligible, but the σ donor ability of the ligand is believed to be augmented upon coordination by a synergistic effect. Back-donation from the metal to the ligand places excess electron density on the ligand which reinforces the ability for the CO to donate σ-electron density. The ability of CO to act as a σ donor is probably more important to the bonding in the $(CN)_5FeCO^{3-}$ complex, where the metal is in a higher oxidation state (formally +2), than in the metal carbonyls, where the metal is in a zero oxidation state. The high oxidation state will be more polarizing and can better accommodate σ donation. This type of synergistic effect should be the most important for small ligands such as CO and CN^-, where the increased ligand electron density due to back-bonding must reside on atoms very close to the metal center. Other π acceptor ligands, such as the aromatic nitrogen heterocycles, have acceptor orbitals that are delocalized over the entire ligand molecule (5–6 atoms). Such delocalization will dissipate any effect the back-donation may have on the σ donor properties. Even so, for Ru(II) back-donation has been shown to significantly increase the σ basicity of coordinated pyrazine at the remote nitrogen atom.[16] The back-bonding and the complementary increase in σ donor ability is expected to be much greater for CO. The result of this increased σ donor ability for CO in $(CN)_5FeCO^{3-}$ is a smaller quadrupole splitting than would be expected for a "π-only" contribution. This brings the data point for CO close to the "σ-only" line even though the bonding of CO is primarily through π acceptance.

Table V. Ligand Affinities

ligand	K_f, M^{-1} Fe(II) $(CN)_5Fe^{3-}$[a]	Fe(III) $(CN)_5Fe^{2-}$[a]	Ru(II) $(NH_3)_5Ru^{2+}$[b]	Ru(III) $(NH_3)_5Ru^{3+}$[b]
CO	$>10^7$	$<10^{-7}$		
pz[c]	9.0×10^5	1.7×10^3		
N_2			3.3×10^4	4×10^{-13}
thiophene			10	2.5×10^{-3}

[a] Reference 9. [b] Reference 17. [c] pz = pyrazine.

Further support for this argument comes from a consideration of the formation constants for the CO and pz complexes of $(CN)_5Fe^{3-}$ and $(CN)_5Fe^{2-}$ as shown in Table V. σ donation dominates the bonding to low-spin Fe(III). The very weak σ base CO has very little affinity for $(CN)_5Fe^{2-}$. Pyrazine, a stronger σ base, has a greater affinity for $(CN)_5Fe^{2-}$ by >10 orders of magnitude. For $(CN)_5Fe^{3-}$ complexes, π back-bonding is much more important and CO, a good π acceptor, forms a very stable complex ($K_f > 10^7$). The π* orbital of pyrazine lies lower in energy than the π* orbital of CO. Despite the π* orbital of pyrazine being at an energy level more favorable for back-bonding (i.e. at an energy closer to that of the metal dπ orbitals), the affinity of pz for $(CN)_5Fe^{3-}$ is 1 order of magnitude less than that of CO. As suggested above, this may be due to the fact that CO has fewer atoms involved in its π system than pz and, as a consequence, the synergistic interaction between the σ- and π-electron density is greater for CO. Additionally, CO has two π orbitals capable of accepting back-donation, while pz has only one. This same reasoning was applied by Kuehn and Taube to a comparison of the affinities of N_2 and thiophene for $(NH_3)_5Ru^{2+}$ and $(NH_3)_5Ru^{3+}$.[17] As shown in Table V, the formation constants for these complexes show the same pattern as was discussed for the iron complexes. Like CO, N_2 is a very weak σ base and strong π acid. From their discussion of K_f values, Kuehn and Taube conclude that if this explanation for the relative affinities observed is correct, "it shows that the so-called synergistic effect, far from being a minor refinement in our ideas of back-donation, is a major effect". The fact that the Mössbauer data also suggest that this may be true indicates that more consideration of the magnitude of the synergistic effect is needed.

The positive slope of the least-squares line in Figure 5 is consistent with the "σ-only" designation. Increasing σ donor ability decreases the center shift and the quadrupole splitting. With this "σ-only" line having been defined with a limited data set, the remaining data were then added to the plot for comparison in Figure 5B. With the exception of NO^+ (which may be considered a special case) the data are clustered relatively close to the line. This tends to indicate that σ effects dominate in determining the quadrupole splitting, since the π effect on the quadrupole splitting opposes that on the center shift and a line of negative slope would result if π effects dominated. As indicated in the figure, ligands that are poorer σ donors and/or better π acceptors are expected to give data points off the line and to the right. The data points for $(CN)_5FeL^{3-}$ complexes that display metal-to-ligand charge transfer (MLCT) absorptions in the visible region are indicated by squares. Circles indicate data points for complexes not having MLCT transitions in the visible region. All of the data points

(15) See, for example, the discussion in: Cotton, F. A.; Wilkinson, G. "Advanced Inorganic Chemistry", 4th ed.; Wiley: New York, 1980; pp 87–90. Tertiary phosphines can form complexes with metals in high oxidation states which show no evidence for π bonding.

(16) Ford, P.; Rudd, D. P.; Gaunder, R.; Taube, H. *J. Am. Chem. Soc.* **1968**, *90*, 1187–1194.

(17) Kuehn, C. G.; Taube, H. *J. Am. Chem. Soc.* **1976**, *98*, 689–702.

for the pyridine and pyrazine derivatives that display MLCT transitions fall to the right of the line. This is consistent with these ligands having π acceptor ability. Qualitatively, there is some agreement between the energy of the MLCT transition and the distance of the Mössbauer data point from the "σ only" line. The complex of the *N*-methylpyrazinium ion, which has the lowest MLCT energy, is the aromatic nitrogen heterocycle farthest from the line. The pyrazine complexes (pyrazine, 2-methylpyrazine, and 2,6-dimethylpyrazine) have data points that lie closer to the line. The complexes of pyridine and 4-methylpyridine, which have the highest MLCT energy, have data points even closer to the line. The agreement is far from perfect, however, with the 4-cyanopyridine complex giving a data point close to the line, contrary to the prediction on the basis of the MLCT energy.

The data for the $(CN)_5Fe^{3-}$ complexes of $AsPh_3$ and $SbPh_3$ fall in the region of the plot indicating π bonding. The data for PPh_3 is on the line, and the data point for $SbPh_3$ is the furthest from it, seemingly indicating a back-bonding order of Sb > As > P. The differentiation between these ligands is surprising, since the back-bonding ability of this series has been described as possibly weak and approximately equivalent.[15]

The complexes of imidazole, 1-methylimidazole, 2-methylimidazole, 4-methylimidazole, and benzimidazole have data points that lie near and to the left of the "σ-only" line. The imidazole complexes do not have a MLCT absorption in the visible region. The Mössbauer data suggest that π back-bonding does not play an important role in the bonding of imidazoles to $Fe(CN)_5^{3-}$. This conclusion was also reached from equilibrium data by Shepherd.[2a] The data point for the histidine complex is to the right of the "σ-only" line. This is probably not due to π bonding but to an additional lattice contribution to the quadrupole splitting arising from the histidine side chain (possibly in the zwitterionic form).

The complexes of the anionic ligands SO_3^{2-} and NO_2^- also give data points to the π-bonding side of the line. These ligands are not expected to have substantial π-bonding capability. The $q_{lattice}$ contribution to the quadrupole splitting would be expected to be greater for an anionic ligand than for a neutral one. Thus, a larger than normal lattice contribution to the quadrupole splitting for the histidine, SO_3^{2-}, and NO_2^- complexes is possible. Internal H bonding may also be a factor for histidine, where the pyrrole hydrogen may interact with the carboxyl group of the side chain.

$(CN)_5FeL^{2-}$ Series. For low-spin Fe(III) complexes the electron density distribution is inherently unsymmetrical due to the singly occupied t_{2g} orbital. In such cases the q_{CF} contribution to the electric field gradient may dominate and obscure the dependence of the quadrupole splitting on the nature of the metal-to-ligand bonding in terms of relative σ or π contributions. In general, the Mössbauer spectra of low-spin Fe(III) complexes show a large temperature dependence. Golding has presented a detailed theoretical treatment of the temperature dependence of the quadrupole splitting of low-spin Fe(III) compounds.[6] Golding's approach has met with only moderate success in treating the Mössbauer data of low-spin Fe(III) complexes.[18] Similar treatments have been presented by Griffith[19] and by Oosterhuis and Lang.[20] These treatments have been applied to Mössbauer spectra of low-spin heme proteins. Although temperature studies were not undertaken in this work, some aspects of Golding's discussion are very useful for interpreting the variations in the quadrupole splittings for different ligands.

(18) (a) Bancroft, G. M.; Platt, R. H. *Adv. Inorg. Chem. Radiochem.* **1972**, *15*, 59–258. (b) Reiff, W. M. *J. Am. Chem. Soc.* **1974**, *96*, 3829–3834.
(19) Griffith, J. S. *Nature (London)* **1957**, *180*, 30–31.
(20) Oosterhuis, W. T.; Lang, G. *Phys. Rev.* **1969**, *178*, 439–456.

Table VI. Mössbauer Data for Low-Spin Fe(III) Complexes

complex	center shift (δ), mm/s	quadrupole splitting (Δ), mm/s	T^d
$K_3Fe(CN)_6$	0.14	0.28[a]	80 K
$Na_2[(CN)_5FeOH_2]$	0.12	1.82	80 K
$Na_2[(CN)_5FeNH_3]$	0.12	1.78	80 K
$Na_2[(CN)_5FePPh_3]$	0.14	1.04	80 K
$Na_2[(CN)_5FeAsPh_3]$	0.20	1.00	80 K
$Na_2[(CN)_5FeSbPh_3]$	0.26	0.94	80 K
$[Fe(phen)_3](ClO_4)_3$	0.31	1.62	rt
$[Fe(4,4'\text{-bpy})_3](ClO_4)_3$	0.32	1.76	80 K
$[Fe(terpy)_2](ClO_4)_3$	0.32	3.43	80 K
$Fe(TPP)(imz)_2$	0.40	2.11[b]	rt
$Fe(Hemin)(imz)_2$	0.41	2.17[b]	rt
$Fe(TPP)(py)_2$	0.43	1.25[b]	LN
$Fe(Hemin)(py)_2$	0.50	1.86[b]	LN
low-spin proteins			
chloroperoxidase (CPO)		2.9[c]	4 K
P-450 2-phenylimidazole		2.85[c]	

[a] Adapted from ref 18a, p 22. [b] Reference 24. [c] Reference 23. [d] Abbreviations: rt = room temperature; LN = liquid-nitrogen temperature (77 K).

If octahedral symmetry is assumed, the electronic ground state of a low-spin d^5 ion is $^2T_{2g}$. In most complexes the degeneracy of this state is completely lifted by a combination of spin–orbit mixing and the crystal field effects. The relative energies of the three states arising from $^2T_2$ can be expressed in terms of three parameters—the spin–orbit coupling constant (λ) and the crystal field distortion parameters ($\hat{\delta}$ and ϵ). Tetragonal distortion is represented by $\hat{\delta}$, and rhombic distortion is represented by ϵ. Golding has shown that the quadrupole splitting is very sensitive to small distortions from octahedral symmetry. The magnitude of Δ is sensitive to the value of $\hat{\delta}$ and ϵ. Golding's evaluation led to a predicted value for the maximum quadrupole splitting (large distortion from octahedral symmetry) as 2.54 mm/s.[6] Under Golding's treatment[6] the distortion parameter is compared as a ratio to the spin–orbit coupling, λ; the latter for Fe(III) is taken to be 400 cm^{-1}. If the distortion is less than $^1/_6$ of the spin–orbit coupling, the quadrupole splitting reaches the constant, maximum value of 2.54 mm/s. The value of Δ is virtually independent of T for values $kT/\lambda \leq 0.5$. Since room temperature has $kT \approx 200$ cm^{-1}, Δ will be independent of T for room temperature and below. Δ becomes a function of T at higher temperatures. Thus quadrupole splittings where $\hat{\delta}$ is less than 70 cm^{-1} will be independent of T below room temperature and may be compared together. In the case of $(CN)_5FeL^{2-}$ complexes, which will differ from C_{4v} geometry only slightly, it is certain that the distortion is within the 70-cm^{-1} limit and should be an excellent test case of the 2.54 mm/s limit. A tetragonal distortion for $(CN)_5FeL^{2-}$ will occur most when L competes with the trans CN^- for π bonding with the Fe(III) center. This prediction agrees remarkably well with the values that appear to define an upper limit of the data set for the $(CN)_5FeL^{2-}$ complexes as shown by Table II and Figure 3.

The $^2T_{2g}$ term for a low-spin d^5 case is split into three levels (E_1, E_2, and E_3) that are close in energy. These energy levels are seen to change from ligand to ligand as indicated by the variations in the quadrupole splitting. For each complex, the observed quadrupole splitting should arise from an interaction between the iron nucleus and an average electric field gradient. The electric field gradient derives from contributions averaged over the three levels—E_1, E_2, and E_3.

The values for the quadrupole splitting for the low-spin $(CN)_5FeL^{2-}$ complexes of Table II may be compared to other available data on low-spin Fe(III) complexes (Table VI). The quadrupole splittings with L = an aromatic N-heterocyclic

ligand are larger than those for other reported complexes. The ligands that approach the upper limit of 2.54 mm/s predicted by Golding are those N-heterocyclic ligands that either have an additional lone pair with the ring structure such as imidazoles and pyrazoles or that have a polarizable lone pair exo to the ring as for the $-NR_2$-substituted pyridines. Interestingly, it is this very same group of ligands whose complexes exhibit the LMCT transition in the $(CN)_5FeL^{2-}$ series. For example, pyridine itself, which lacks an internal or exo lone pair of electrons, does not exhibit the LMCT transition in its $(CN)_5Fe(py)^{2-}$ complex. In concert, the quadrupole splitting parameter of 2.12 mm/s falls on the approximate line in which Δ increases by the σ-only donation (i.e. roughly proportional to the affinity of a given ligand for a proton). Since the quadrupole splitting reflects nuclear interaction of the electronic ground state while the LMCT transition implies the accessibility of an electron excited state, it may be worth commenting on why the same type ligands give rise to the phenomena. In the limit of Golding's treatment the sixth ligand L must be sufficiently different from the five CN^- ligands to achieve a large distortion from octahedral symmetry. This criteria will be met if a ligand is a much better π donor toward Fe(III) of $(CN)_5FeL^{2-}$ than CN^-. The same electron-rich ligands are necessary for the Fe(III) center to be sufficiently oxidizing to serve as an electron acceptor in the excited state of the LMCT transition.

Experimental Section

Mössbauer-Effect Spectroscopy. The Mössbauer spectra were obtained with a scanned-velocity spectrometer operating in the time mode. The source was driven by a triangular wave output from a NSEC Model AM-1 Mössbauer-effect spectrometer control unit. The source is attached to a rod that is axially mounted between two permanent magnets and voice coils: one as an electromechanical transducer to drive the source, the other for feedback to the control unit. The ^{57}Co source was in a rhodium matrix. The source and absorber were at room temperature. A gas-filled (74% Kr/3% CO_2) proportional counter tube with a beryllium entrance window was used as the detector. The output of the detector was amplified with the following: (1) an Ortec preamplifier, Model 109PC, (2) an Ortec active filter amplifier, Model 435, and (3) an Ortec single-channel analyzer, Model 406A. A Tracor-Northern NS-900 multichannel analyzer was used to store the counting information. A minimum of 1.5×10^6 counts at the peak channel were stored per complex. A final record of the spectrum could be obtained with a teletype readout. Alternately, the readout could be stored directly on 5-in floppy disks through an Apple II computer. Peak positions were also determined directly from the oscilloscope display of the multichannel analyzer. The velocity scale and isomer shift references were obtained by periodic calibration with a sodium nitroprusside (NP) absorber standard. Line widths for NP were typically 0.27 mm/s. Those of the complexes varied from 0.4 to 0.7 mm/s with a representative value of 0.43 mm/s. Sample thickness was $\sim$3 mm.

Syntheses. The Fe(II) complexes, $(CN)_5FeL^{3-}$, were prepared according to published procedures.[4,7] $Na_3(CN)_5FeNH_3 \cdot 3H_2O$[21] served as the starting material for all complexes. The imidazole complexes were prepared in the presence of a small amount of ascorbic acid to prevent air oxidation. The Na^+ or K^+ salts were prepared by precipitation with ethanolic solutions of NaI or KI. Precipitation of the imidazole complexes by $(NH_3)_5Co(imz)^{3+}$, $Ru(NH_3)_6^{3+}$, or $Co(NH_3)_6^{3+}$ was achieved by addition of a solution of the Cl^- or ClO_4^- salts of these cations to a solution of the $(CN)_5FeL^{3-}$ complex. The precipitate forms immediately and is exceedingly insoluble in water.

The Fe(III) complexes, $(CN)_5FeL^{2-}$, were prepared by oxidation of a solution of the corresponding Fe(II) complex. The imidazole and pyrazole complexes were prepared by oxidation with H_2O_2.[1,2] Oxidation of the complexes of the pyridines and pyrazines was achieved by bubbling a stream of Cl_2 gas through the solution. Attempts at precipitating the Na^+ salts of these complexes by the addition of large volumes of cold ethanol followed by ethanol/ether mixtures resulted in the formation of oils. The solvent was decanted, and the oil was washed repeatedly with acetone while the side of the beaker was scratched. On days of low humidity, a solid could be obtained by this method. Ca^{2+} salts of these complexes were obtained by adding one volume of a nearly saturated solution of $CaCl_2$ to the reaction mixture. Slow evaporation (1–2 weeks) resulted in the formation of a crystalline product. Addition of a solution of $ZnCl_2$ to a solution of the $(CN)_5FeL^{2-}$ complex resulted in the immediate precipitation of the insoluble Zn^{2+} salt. Precipitation with $(CH_3)_2Dabco^{2+}$ (*N*,*N'*-dimethyl-1,4-diazoniabicyclo[2.2.2]octane ion) ion)[22] was achieved by dissolving the $Na_2(CN)_5FeL \cdot xH_2O$ complex in an aqueous solution containing an excess of $(CH_3)_2DabcoI_2$ and reprecipitating with cold ethanol. The identities of all complexes were verified by reducing the complex with ascorbic acid and comparing the UV–visible spectrum with that of a solution of the Fe(II) complex prepared directly. Spectra were obtained on a Varian-Cary 118C spectrophotometer. Characterizations of complexes were as described previously in literature references contained in the cited papers.[1,2,7,8]

Acknowledgment. The authors are grateful for support of this work through the National Science Foundation (Grant No. CHE 802183). We are also indebted to Professor Darel K. Straub for use of his Mössbauer apparatus and for helpful discussions.

Registry No. $K_3(CN)_5Fe(imz)$, 69480-69-9; $K_3(CN)_5Fe(1\text{-}CH_3imz)$, 87336-58-1; $K_3(CN)_5Fe(2\text{-}CH_3imz)$, 87336-59-2; $K_3(CN)_5Fe(4\text{-}CH_3imz)$, 87336-60-5; $Na_3(CN)_5Fe(l\text{-histidine})$, 87336-61-6; $Na_3(CN)_5Fe(benzimidazole)$, 87336-62-7; $Na_3(CN)_5Fe(hypoxanthine)$, 87336-63-8; $K_3(CN)_5Fe(4\text{-}NO_2imz)$, 87336-64-9; $[(NH_3)_5Co(imz)][(CN)_5Fe(imz)]$, 87336-65-0; $[Ru(NH_3)_6][(CN)_5Fe(imz)]$, 73635-17-3; $[Co(NH_3)_6][(CN)_5Fe(2\text{-}CH_3imz)]$, 87336-66-1; $Ca(CN)_5Fe(imz)$, 87336-67-2; $Zn(CN)_5Fe(imz)$, 87336-85-4; $Ca(CN)_5Fe(1\text{-}CH_3imz)$, 87336-68-3; $Zn(CN)_5Fe(1\text{-}CH_3imz)$, 87336-86-5; $Ca(CN)_5Fe(2\text{-}CH_3imz)$, 87336-69-4; $[(CH_3)_2dabco][(CN)_5Fe(2\text{-}CH_3imz)]$, 87336-87-6; $Ca(CN)_5Fe(4\text{-}CH_3imz)$, 87336-70-7; $Ca(CN)_5Fe(1,2\text{-}(CH_3)_2imz)$, 87336-71-8; $Na_2(CN)_5Fe(benzimidazole)$, 87336-72-9; $Na_2(CN)_5Fe(pyz)$, 87336-73-0; $Na_2(CN)_5Fe(3,5\text{-}(CH_3)_2pyz)$, 87336-74-1; $Na_2(CN)_5Fe(4\text{-}((CH_3)_2N)py)$, 87336-75-2; $Na_2(CN)_5Fe(4\text{-}(NH_2)py)$, 87336-76-3; $[(CH_3)_2dabco][(CN)_5Fe(4\text{-}CH_3py)]$, 87336-77-4; $Ca(CN)_5Fe(py)$, 87336-78-5; $Na_2(CN)_5Fe(py)$, 70348-30-0; $[(CH_3)_2dabco][(CN)_5Fe(py)]$, 87350-58-1; $[(CH_3)_2dabco][(CN)_5Fe(4\text{-}C(O)CH_3py)]$, 87336-80-9; $Na_2(CN)_5Fe(4\text{-}C(O)NH_2py)$, 87336-81-0; $[(CH_2)_2dabco][(CN)_5Fe(pyridazine)]$, 87350-57-0; $Na_2(CN)_5Fe(4\text{-}CH_3py)$, 87336-82-1; $Na_2(CN)_5Fe(4\text{-}COOHpy)$, 87336-83-2; $Na_2(CN)_5Fe(2\text{-}CH_3pyr)$, 87336-84-3; $Na_2(CN)_5Fe(pyr)$, 84711-79-5; $[(CN)_5Fe(pyCO_2)]^{4-}$, 37475-64-2; $[(CN)_5Fe(2\text{-methylpyrazine})]^{3-}$, 76299-52-0; $[(CN)_5Fe(2,6\text{-dimethylpyrazine})]^{3-}$, 87336-88-7; $[(CN)_5Fe(4,4'\text{-bipyridine})]^{3-}$, 37475-72-2; $[(CN)_5Fe(4\text{-}C(O)NH_2py)]^{3-}$, 40299-77-2; $[(CN)_5Fe(4\text{-}CNpy)]^{3-}$, 62704-26-1.

(21) Brauer, G. "Handbook of Preparative Inorganic Chemistry", 2nd ed.; Academic Press: New York, 1965; Vol. 2, p 1511.

(22) Oea, S.; Hovaith, B.; Zalut, C.; Harris, R. *J. Org. Chem.* **1959**, *24*, 1348–1349.

(23) Münck, E. In "The Porphyrins"; Dolphin, D., Ed.; Academic Press: New York, 1979; Vol. IV, Chapter 8.

(24) Epstein, L. M.; Straub, D. K.; Maricondi, C. *Inorg. Chem.* **1967**, *6*, 1720–1724.